

## Article

# Statistical Modeling of Fine Sediments Dredged Using a Variable Area Dredging Suction Head to Improve Water Quality

Leigh A. Provost <sup>1,†</sup>, Robert Weaver <sup>1</sup> and Nezamoddin N. Kachouie <sup>2,\*</sup>,<sup>†</sup>

<sup>1</sup> Department of Ocean Engineering and Marine Sciences, Florida Institute of Technology, Melbourne, FL 32901, USA; lprovost2013@my.fit.edu (L.A.P.); rjweaver@fit.edu (R.W.)

<sup>2</sup> Department of Mathematical Sciences, Florida Institute of Technology, Melbourne, FL 32901, USA

\* Correspondence: nezamoddin@fit.edu

† Both authors has equal contribution.

**Abstract:** The changing climate affects the agricultural lands, and, in turn, the changes in agricultural lands alter the watershed. A major concern regarding waterbodies is the increased sedimentation rates due to climate change. To improve the water quality, it is crucial to remove fine sediments. Using current environmental dredging methods is challenging because of the sediment volumes that must be dredged, the absence of nearby disposal sites, and the shoreline infrastructure at the dredging locations. To address these issues, we used a surgical dredging method with a variable area suction head that can easily maneuver around the docks, pilings, and other infrastructures. It can also isolate the fine grain material to better manage the dredged volumes in the seabed where nutrients are typically adhered. To this end, a statistical analysis of the dredged samples is essential to improve the design efficiency. In this work, we collected several samples using a variable area suction head with different design settings. The collected samples using each design setting were then used to model the distributions of the different grain sizes in the dredged sediments. The proposed statistical model can be effectively used for the prediction of sediment sampling outcomes to improve the gradation of the fine sediments.

**Keywords:** dredging; water quality; statistical modeling; log-normal distribution; beta distribution; bootstrap method



**Citation:** Provost, L.A.; Weaver, R.; Kachouie, N.N. Statistical Modeling of Fine Sediments Dredged Using a Variable Area Dredging Suction Head to Improve Water Quality. *Hydrology* **2021**, *8*, 98. <https://doi.org/10.3390/hydrology8030098>

Academic Editors: James E. Ball and Tommaso Moramarco

Received: 15 April 2021

Accepted: 15 June 2021

Published: 28 June 2021

**Publisher's Note:** MDPI stays neutral with regard to jurisdictional claims in published maps and institutional affiliations.



**Copyright:** © 2021 by the authors. Licensee MDPI, Basel, Switzerland. This article is an open access article distributed under the terms and conditions of the Creative Commons Attribution (CC BY) license (<https://creativecommons.org/licenses/by/4.0/>).

## 1. Introduction

The potential for higher sedimentation rates in waterbodies is a growing concern stemming from climate change [1]. The projected impacts of our changing climate raise concerns regarding associated changes in agricultural lands and the effects those changes may have on the watershed. Some of these projected impacts include changes in rainfall patterns, desertification, land usage, and runoff [2]. The National Oceanic and Atmospheric Administration's (NOAA) National Climate Report produced the map [3] shown in Figure 1, illustrating precipitation patterns in the United States in 2017 in comparison with the average precipitation patterns over 122 years starting from 1895.

The map shows that more than half of the states in the continental US experienced above average precipitation. NOAA ranked the year 2017 the 3rd warmest and the 20th wettest year on record, with precipitation being above average for the five consecutive preceding years.

Climate change simulations for the Beasley Lake watershed in Mississippi utilizing the AnnAGNPS pollution model suggested increases in agricultural pollutant loading to be between 9% and 12% by 2070 [4]. Similarly, in the Apalachicola area of Florida, a Soil and Water Assessment Tool was developed [5] to simulate sediment loading with regard to climate conditions of the year 2000 and the year 2100. It showed that climate change may have seasonal impacts on runoff and sediment loading, affecting the seasonal patterns of plant and animal life in the waterway [5]. Beyond the US, models have predicted a

3.3%–16.5% increase in phosphorous loading in Danish streams within the next 100 years varying by region, thus negatively altering the ecology of most lakes [6]. Various models have shown similar results in a number of locations [7,8].

Nutrients carried in the runoff in the form of fertilizer or organic material is one of the causes of eutrophication of our coastal waterbodies. As the organic matter decays and mixes with the fine sediments, muck is formed. Muck is fine-grained sediment characterized by having high organic nutrients and high water content [9–12]. The nutrient load that is constantly fluxing up into the water from the muck can be higher than the nutrients flowing into the water body from the runoff [13]. This legacy loading of nutrients is an additional cause of eutrophication. The increase in nutrient loading in water systems has severe impacts on ecosystems, such as triggering algal blooms that then cause low dissolved oxygen and result in massive fish kills, such as those seen in recent years in the Indian River Lagoon [14,15].

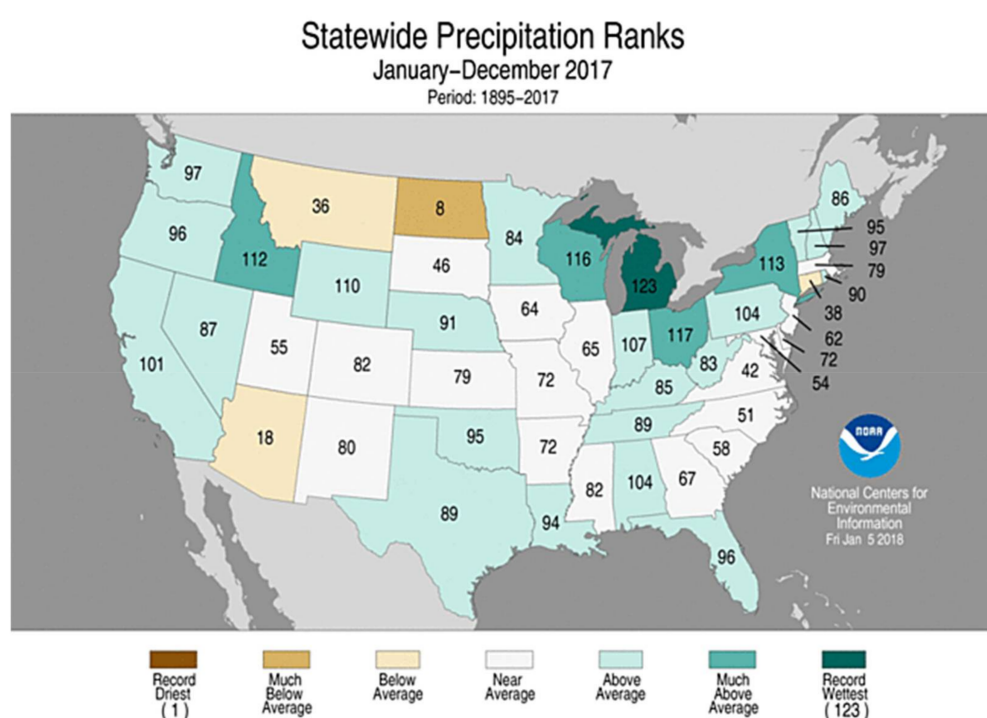


**Figure 1.** Statewide precipitation, 2017 [3]. Ranks are from 1 for driest to 123 for wettest.

In addition to trapping nutrients, fine sediments are also a source of turbidity. Due to the fine-grained nature of the silts and clays that make up the muck, it is easily mixed up into the water column, releasing nutrients and limiting light availability. The increased turbidity decreases photosynthetic growth, and as the fine material resettles, the natural substrate of the lagoon can become covered [14]. The removal of fine sediments is crucial to improve water quality. Muck poses a threat to communities that rely on the natural physiology of the lagoon: a sandy substrate, steady nutrient cycles, and clear water.

The primary existing method for reducing nutrients and nutrient loading to eutrophic systems beyond agricultural mitigation is the use of environmental dredging, which is defined as “the removal of contaminated sediments from a waterbody for purpose of sediment remediation” [16,17]. Conventional methods use cutter suction or hydraulic suction dredges that require significant processing times and can alter or damage the benthos [18]. Due to the volumes that must be dredged and the locations of the areas that require dredging, current environmental dredging methods often face challenges in meeting the Army Corps’ guidelines, such as the availability of a nearby disposal site or the shoreline infrastructure. To address this issue, a “surgical dredging” method was

established by use of a variable area suction head [19,20]. The research presented in this paper is focused on the removal of fine sediments with minimal disturbance to the natural substrate by testing the design of a variable intake suction head for the hydraulic dredging of fine sediments. Using a variable area suction head can facilitate maneuvering of a small hydraulic dredge around the docks, pilings, and other infrastructures. It can also pinpoint the fine-grained and nutrient-laden sediments in the seabed to better manage the dredged volumes. However, current resources limit the ability to fully analyze the design efficiency. A statistical method is essential to further improve the previous design and to avoid the significant processing power required for performing a full sediment flow analysis on the suction head. In this paper, a statistical model is introduced for the prediction of sediment sampling outcomes to improve the gradation of the fine sediments.

## 2. Background

The variable area suction head, depicted in Figure 2, was tested at the Florida Institute of Technology using a 5' × 5' cylindrical tank with a pumping arrangement.



**Figure 2.** Variable area suction head (with and without gearbox cover, shown left to right).

During each dredging test, the suction head was set to three different opening settings, 5/8", 2.5", and 5", which were referred to as closed, halfway, and open, respectively. These settings are in reference to the spacing of the bottom and the top plates of the suction head. Control tests were also performed using just the hose alone with no suction head attached.

With these heights, the intake area of the suction head was calculated by using the following equation for the surface area:

$$A_i = 2\pi rh \quad (1)$$

Using the calculated intake areas, the intake velocity was calculated for each setting using the continuity equation.

$$Q = V_i A_i \quad (2)$$

The flow,  $Q$ , for all tests was set at 120 GPM. The calculated values for the intake area and the intake velocity are shown in Table 1.

**Table 1.** Intake areas and velocities.

	Control	Closed	Halfway	Open
Intake Area (cm <sup>2</sup> )	45.60	228.02	912.07	1824.15
Intake Velocity (cm/s)	166.01	33.20	8.30	4.15

When the intake velocity for each setting was established, the expected sediment diameter to be entrained by the suction head was calculated. For dredging when no jet systems were being used, the seabed was assumed to be in a stable state, so no particles were suspended. With this assumption, the Shields parameter,  $\Psi$ , can be used to find the

sediment diameter for which movement is expected. The Shields parameter is expressed as a ratio of the liberating moment to the restoring moment [21]:

$$\Psi = \frac{\tau_c}{(\rho_s - \rho)gd} \quad (3)$$

where  $\rho_s$  is the density of the sediment,  $\rho$  is the density of the fluid (water),  $d$  is the characteristic sediment diameter,  $g$  is the acceleration due to gravity, and dimensional shear stress  $\tau_c$  is

$$\tau_c = \frac{1}{2}\rho C_D u^2 \quad (4)$$

where  $u$  is the intake velocity, and  $C_D$  is the drag coefficient [21]:

$$C_D = \frac{24}{Re} \sqrt{\left(1 + \frac{3Re}{16}\right)} \quad (5)$$

where  $Re$  is Reynolds number:

$$Re = \frac{\rho w d}{\mu} \quad (6)$$

where  $w$  is the fall velocity of the sediment [21]:

$$w = \sqrt{\frac{4(\rho_s - \rho)gd}{3\rho C_D}} \quad (7)$$

and  $\mu$  is the viscosity. Solving Equation (3) for  $d$ , we have

$$d = \frac{\tau_c}{\Psi(\rho_s - \rho)g} \quad (8)$$

Alternatively, sediment diameters can be expressed by [21]

$$\varphi = -\log_2 d \quad (9)$$

A Shields parameter of 0.03 is a typical value for incipient sediment motion [21], and using the density of quartz  $2.65 \frac{\text{g}}{\text{cm}^3}$ , the drag coefficient for an imperfect sphere is approximately 0.44. Using the values above in Equation (8), the sediment size properties are shown in Table 2.

**Table 2.** Sediment diameter for incipient motion.

	Control	Closed	Halfway	Open
$d$ (mm)	1299.54	51.98	3.25	0.81
$\varphi$	-10.34	-5.70	-1.70	0.30

In practice, the suction head does not necessarily entrain the calculated sediment size. The fall velocities of the sediment can be used to approximate the entrained sediment size. A particle will be entrained if the fall velocity of the particle is smaller than the intake velocity of the suction head. To calculate  $d$  using the fall velocity, Equation (7) can be solved for  $d$ :

$$d = \frac{w^2 3\rho C_d}{4(\rho_s - \rho)g} \quad (10)$$

The expected entrained sediment diameter of the particles that are suspended directly at the intake of the dredging head are calculated iteratively using Equation (10) (Table 3).

These values are the approximated sediment sizes expected in the dredge slurry. The approximated sediment sizes along with the collected samples in the previously ran tests

can be used in a statistical model to estimate the entrained sediment sizes and improve the efficiency of the suction head design.

**Table 3.** Sediment diameter for entrainment.

	Control	Closed	Halfway	Open
$d$ (mm)	22.44	2.67	0.57	0.30
$\varphi$	−4.49	−1.42	0.82	1.73

### 3. Methods

To estimate the entrained grain size and predict the entrained percentage of a given grain size based on the total sample weight, the collected samples during the test runs were used to model the probability distribution of the grain size based on the suction head's parameters. Log-normal distribution has been commonly used for grain size analysis, as it is outlined in the Coastal Engineering Manual [22]. First, the grain size distribution is modeled by a log-normal distribution [23]. Then, the probability of a specific grain size is estimated using the beta distribution. The beta distribution is theoretically appealing to model the percentage of sediment weights of different grain sizes. The number of collected samples in the test runs is small due to the time required to acquire and process a sample. Therefore, a bootstrap method was employed to estimate an empirical beta probability distribution.

#### 3.1. Log-Normal Model of Grain Size

In the first test run, the so-called no shroud test, the suction head operated alone without any additional jetting system or shroud configuration. Separate tests were run, and we collected 3 samples for each setting of the suction head. These samples were then analyzed in the lab by using a sieving technique. The weight of each grain size was measured (in a sediment sample), and its percentage was calculated. The mean grain size (in  $\varphi$ ) can be estimated by [23]

$$M_{d\varphi} = \frac{\varphi_{16} + \varphi_{84}}{2} \quad (11)$$

where  $\varphi_{16}$  and  $\varphi_{84}$  are the 16th and 84th grain size percentiles measured in  $\varphi$ . The standard deviation of the grain size (measured in  $\varphi$ ) can be approximated by

$$\sigma_{\varphi} = \frac{\varphi_{84} - \varphi_{16}}{2} \quad (12)$$

Skewness  $\alpha_{\varphi}$ , second skewness  $\alpha_{2\varphi}$ , and kurtosis (peakedness)  $\beta_{\varphi}$  of the grain size are [23]

$$\alpha_{\varphi} = \frac{M_{d\varphi} - \varphi_{50}}{\sigma_{\varphi}} \quad (13)$$

$$\alpha_{2\varphi} = \frac{\frac{1}{2}(\varphi_5 + \varphi_{95}) - M_{d\varphi}}{\sigma_{\varphi}} \quad (14)$$

$$\beta_{\varphi} = \frac{(\varphi_{16} - \varphi_5) + (\varphi_{95} - \varphi_{84})}{2\sigma_{\varphi}} \quad (15)$$

#### 3.2. Beta Distribution for Proportion of Grain Size

The beta distribution is a continuous probability distribution defined on the interval [0,1]. It is parameterized by two positive shape parameters  $\alpha$  and  $\beta$  to control the shape of the distribution. The beta distribution can be applied to model random variables in a broad range of different disciplines. Beta distribution is suitable to model random variables with intervals of finite length. Hence, it has been commonly used to model the random behavior

of proportions, fractions, and percentages. In turn, beta distribution is a natural choice to model the percentage of the sediment weights of the different grain sizes in this project.

The proportion of grain size based on the total sample weight can be modeled using the beta distribution [24]:

$$f(g) = \frac{g^{\alpha-1} (1-g)^{\beta-1}}{\Gamma(\alpha)\Gamma(\beta)} \Gamma(\alpha + \beta) \quad (16)$$

where  $g$  is the grain size,  $\alpha$  and  $\beta$  are the shape factors, and  $\Gamma$  is the Gamma function. Parameters of the beta distribution ( $\alpha$  and  $\beta$ ) are defined by the moments (mean and standard deviation) of distribution [25]:

$$\begin{aligned} \alpha &= \left( \frac{1-\mu}{\sigma^2} - \frac{1}{\mu} \right) \mu^2 \\ \beta &= \alpha \left( \frac{1}{\mu} - 1 \right) \end{aligned} \quad (17)$$

In practice, parameters of the beta distribution ( $\alpha$ ,  $\beta$ ) can be estimated using the sample mean ( $\bar{g}$ ) and sample variance ( $S_g^2$ ) of the collected sample:

$$\begin{aligned} \hat{\alpha} &= \left( \frac{1-\bar{g}}{S_g^2} - \frac{1}{\bar{g}} \right) \bar{g}^2 \\ \hat{\beta} &= \hat{\alpha} \left( \frac{1}{\bar{g}} - 1 \right) \end{aligned} \quad (18)$$

### 3.3. Bootstrap Analysis

A sample size of at least 30 is recommended for a sound estimate [26]. The collected sample size in this work was three for each setting. Therefore, a bootstrap analysis on the data was performed to generate a large bootstrap sample size to perform the analysis. A beta distribution was then estimated for the generated bootstrap sample and compared to the previously estimated beta distribution from the original samples. The estimated shape parameters of the beta distribution can be used for predicting sediment distribution for a specific design set and to identify the optimal design setting of the suction head for the expected results.

First, 3 sediment weights were combined for each grain size (combined sediment sample), and then bootstrap samples were generated by resampling (with replacement) the combined sample for each grain size 5000 times. In this way, a total of 7 sets (of 5000 samples) were generated for each of the suction settings. For each grain size, the sums of the 3 resamples were taken. Then, those sums of each grain size were summed together to obtain a series of bootstrapped sample weights. The sums for each respective grain size were then divided by the bootstrapped sample weight to obtain a bootstrap proportion. The bootstrap proportion provides an estimate of the weight proportion of each grain size in the sample for different settings. The bootstrap analysis was performed by resampling the measured weight of each individual grain size 5000 times as depicted in Table S1 for the control sample with a grain size of phi equal to zero (1 mm).

Next, each row of resampled data was summed over each of the 7 grain sizes. This provided a 5000 by 7 matrix. The rows were then summed to obtain the total sample weight for all grain sizes of each resample (Table S2). Finally, to quantify the bootstrap proportions, the sum of each grain size for each resample was divided by its respective total sample weight as depicted in Table S3. For example, resample 1 in this table shows that a grain size with phi = 0 makes up 0.93% of the sample, whereas a grain size with phi = 1.23 makes up 15% of the total sample weight.

## 4. Results and Discussion

Because the collected samples for each setting are of a small size, to better visualize the sediment distribution, the total weights of three samples for the same setting were combined to create one larger sample for that specific setting. The 16th and 84th percentile

of the distribution ( $\varphi_{16}$  and  $\varphi_{84}$ ) in Equation (12) were then interpolated from the  $\varphi$  plot and solved to find the mean grain size for each setting.

#### 4.1. Log-Normal Statistics

The estimated parameters for the log-normal distribution are summarized in Tables 4 and 5. Table 4 shows the estimated parameters for each sample individually, while Table 5 shows the estimated parameters for the combined samples. The sediments with smaller diameters are represented by a larger  $\varphi$  value in the  $\varphi$  scale in these tables.

**Table 4.** Estimated parameters for the no shroud test.

	$M_{d\varphi}$	$\sigma_\varphi$	$\alpha_\varphi$	$\alpha_{2\varphi}$	$\beta_\varphi$
Control 1	1.39	0.798	−0.189	−0.015	0.607
Control 2	1.682	0.897	−0.05	0.177	0.891
Control 3	2.398	1.742	0.32	−0.106	0.178
Closed 1	2.149	1.55	0.043	NA	NA
Closed 2	2.421	1.535	0.378	−0.142	0.314
Closed 3	1.656	1.021	−0.046	0.419	0.994
Halfway 1	1.958	0.636	−0.07	−0.401	1.184
Halfway 2	2.706	1.248	0.284	−0.252	0.464
Halfway 3	2.023	0.998	0.004	0.132	1.012
Open 1	2.757	1.258	0.313	−0.21	0.378
Open 2	2.005	0.67	−0.099	−0.279	1.107
Open 3	2.738	1.289	0.304	NA	NA

**Table 5.** Estimated parameters of the no shroud test for combined samples.

	$M_{d\varphi}$	$\sigma_\varphi$	$\alpha_\varphi$	$\alpha_{2\varphi}$	$\beta_\varphi$
Control	2.354	1.712	0.3719	−0.0944	0.372
Closed	2.048	1.377	0.1691	0.0395	0.1690
Halfway	2.1310	0.861	0.05	0.0671	0.050
Open	2.2680	0.861	0.0361	0.0618	0.036

As it can be seen in Table 4, excluding the control, the largest mean grain size (smallest mean  $\varphi$  value) is obtained in the third sample of the closed setting, and the smallest mean grain size (largest mean  $\varphi$  value) is obtained in the first sample of the open setting. Similarly, with the combined samples (Table 5), the smallest mean  $\varphi$  value is obtained in the closed setting, and the largest mean  $\varphi$  value is obtained in the open setting. These results demonstrate that the mean grain size being reduced as the opening size increases holds true.

When comparing Tables 4 and 5, it may be noticed that there are some discrepancies between the values presented in the individual samples versus their combined version. As an example, if the reader were to average the  $M_{d\varphi}$  values of the control samples in Table 4, this value would not be the same as the value represented in Table 5. This discrepancy occurs because the physical weight of each individual sample (i.e., control 1, control 2, and control 3) used to determine this value varies. Thus, numerically, each sample is weighted differently in the combined calculations.

The standard deviation ( $\sigma_\varphi$ ) in the  $\varphi$  value represents the gradation of a sediment sample. A perfectly sorted sample would have a standard deviation of 0. The standard deviation of a well-sorted sample would be less than or equal to 0.5, and the standard deviation of a poorly sorted sample would be larger than or equal to 1 [21]. In Table 5, the largest standard deviation, so the most poorly sorted sample, belongs to the control test. This is followed by the closed setting. The gradation of the sample improved by nearly 50% by the halfway and open settings with the same standard deviation of 0.861; however, none of these settings (halfway and open) are considered “well-sorted” by definition. This shows

that as the opening size of the suction head is increased, the sediment size gets closer to the mean grain size, whereas in the control test, the sediment size is either much larger than or much smaller than the mean grain size. This is further investigated by the skewness ( $\alpha_\varphi$ ) of the sample in which the separation of the mean grain size from the median grain size is evaluated. A positive value of  $\alpha_\varphi$  is indicative of distributions skewed toward higher  $\varphi$  values (longer right tail), and a negative value is indicative of a skew toward smaller  $\varphi$  values (shorter right tail), with the value of zero representing a perfectly symmetrical distribution [23]. As seen in Table 5, the largest skew value belongs to the control test and, since it is a positive value, this demonstrates the skewness is toward higher  $\varphi$  values, or smaller sediment diameters. This skewness then reduces as the suction head is opened toward a more symmetrical distribution with the open setting having an  $\alpha_\varphi$  value of 0.0361.

#### 4.2. Beta Distribution for the Analysis of Sediment Weight

A beta distribution was utilized to demonstrate the percentage of sediment weight. Its parameters were estimated using the collected samples for each design setting. The cumulative distribution function (CDF) and probability density function (PDF) were then estimated and visualized for each test. Moreover, the PDF and CDF of the bootstrapped data were estimated and visualized. The sediment size demonstrated in the figures based on the  $\varphi$  values are summarized in Table 6.

**Table 6.** Sediment size and associated  $\varphi$  values.

$\varphi$	Sediment Size
$\varphi \leq 0$	Very Large
$0 < \varphi \leq 1.23$	Relatively Large
$1.23 < \varphi \leq 2$	Large
$2 < \varphi \leq 2.74$	Medium
$2.74 < \varphi \leq 3.24$	Small
$3.24 < \varphi \leq 4$	Relatively Small
$4.32 \leq \varphi$	Very Small

Figure 3 shows the PDF and CDF of the beta distribution for the original samples as well as the bootstrap sample of the control test. Heatmaps for the original samples as well as the bootstrap sample of the control test are depicted in Figure 4. The fraction of the sample weight for small, relatively small, and very large grain sizes is almost zero (Figures 3 and 4). The fraction of the sample weight for the very small and large grain size is up to 60%, while the fraction of the medium size and relatively large grain size is up to 30%. The fraction of the sample weight for the very small grain size is between 5% and 60%, for the medium size is between 10% and 30%, for the large size is between 20% and 60%, and for the relatively large size is between 20% and 30%. As demonstrated in Figure 4, the medium, large, and relatively large sediment sizes made up more of the sample weight. Comparing this to the bootstrapped data, some similarities are observed. However, the densities of the data are less extreme, and the curves of the mid-range sediment sizes (medium, large, and relatively large) and the very small sediment size have stretched over a broader range. For example, the medium grain size was originally peaked somewhat steeply at around 25% of the total sample weight, while the tails of the curve asymptote to 0 at around 10–30%. However, comparing the same grain size of the bootstrapped data, the density peaks at around 15% of the total sample weight, while the tails span from 0% to around 35%. The PDFs for the same control test show that the very small or very large grain size will make up less of the sample, while the coarser size is more likely to make up a larger fraction of the sample. Similar results are interpreted from the bootstrap PDF. However, just as the bootstrap CDFs were stretched over the x-axis, the bootstrap PDFs are demonstrating a similar stretch over the x-axis. This shift means that of the bootstrapped data, the grain sizes are more likely to make up a larger range of the total sample. For example, the distribution of the original sample shows that the relatively large grain size

has less than 10% probability of making up 20% of the total sample weight, while the bootstrap distribution data suggest a 30% chance of the relatively large grain size making up the same fraction of the sample (20% of the total sample weight).

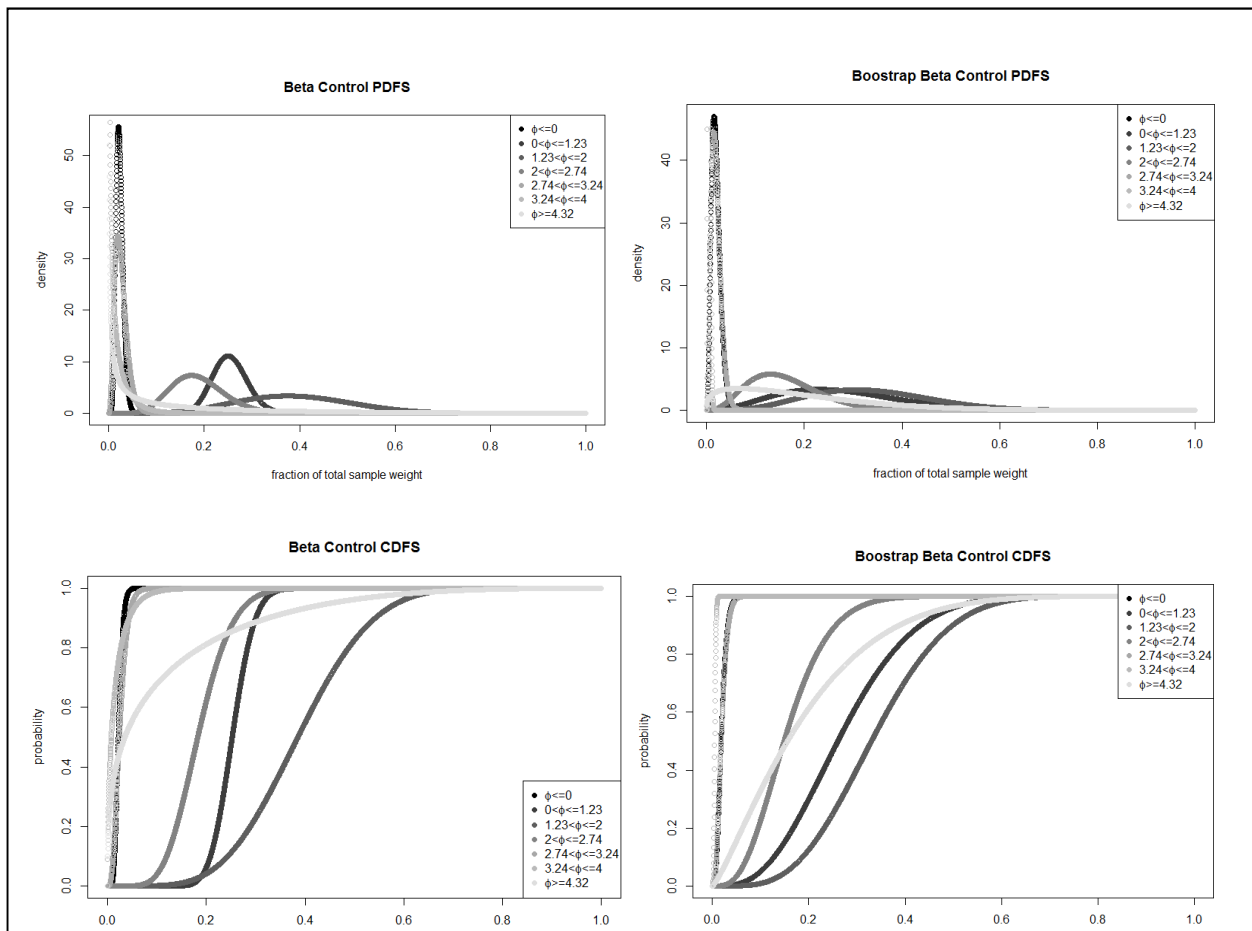


Figure 3. Control test—beta distributions of original samples along with bootstrap distributions.

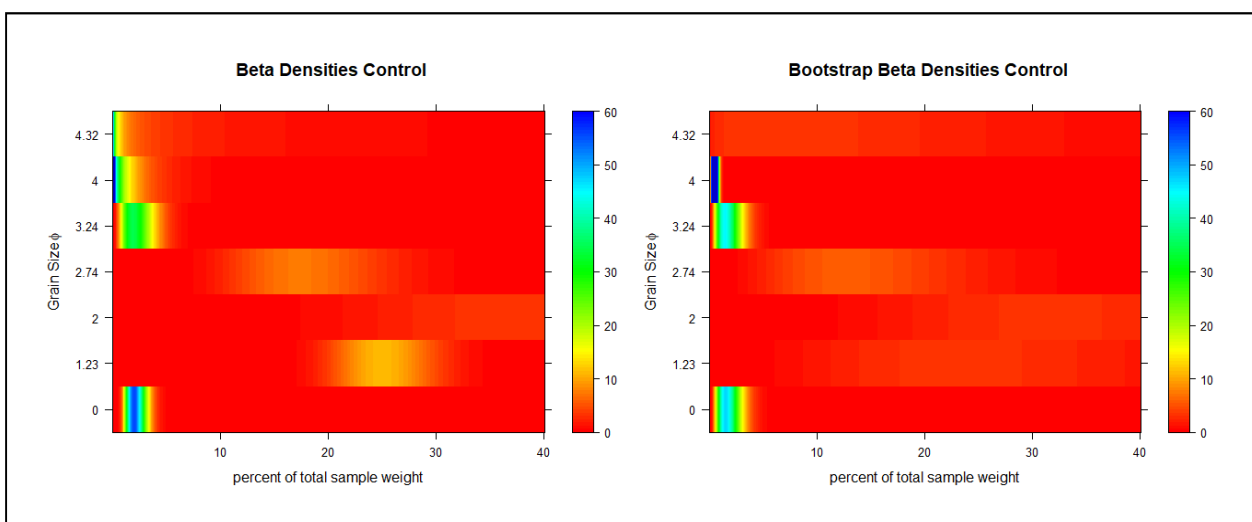
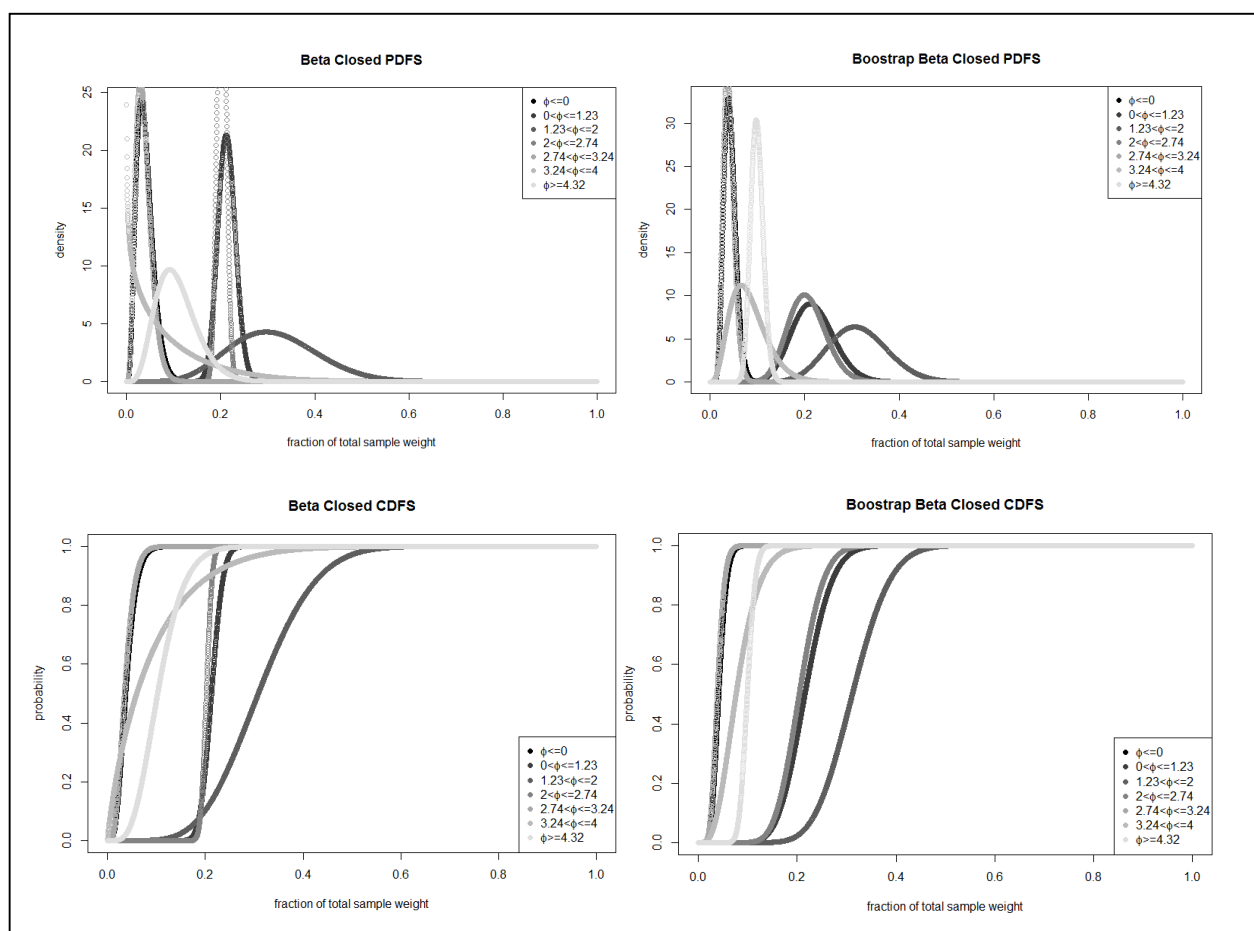


Figure 4. Control test—heat maps of original samples and bootstrap samples.

The results regarding the closed test exhibited much different results compared to the control group. Figures 5 and 6 show the weight distribution for the closed setting. The

distributions of the smaller grain sizes make up slightly more of the total sample weight in comparison with that of the control (close to zero). Similar to the control sample, the bootstrap distributions of the smaller grain sizes in the closed setting exhibited a spreading out along a larger fraction of the total sample weight. This can be seen more clearly in the comparison of the CDFs of the original sample and the bootstrapped one. For example, the distribution of the original sample shows that there is approximately a 20% chance that the relatively large grain size makes up 20% of the sample weight, while it is closer to 30% in the bootstrap distribution. Overall, looking at the distributions of the samples taken with the closed setting, the larger grain sizes were more likely to make up more of the sample weight. The smaller grain sizes also have a higher chance (although not likely) of making up slightly larger portions of the sample weights as compared to those of the control test. The results agree with the estimated log-normal distribution summarized in Table 5, which shows that the closed test has a mean grain size much larger than that of the control test.



**Figure 5.** Closed design setting—beta distributions of original samples along with bootstrap distributions.

Moving on to the halfway test (Figures 7 and 8), the differences in the distributions are more visible in comparison with both the control and closed settings. In the halfway setting, the distribution of the largest (very large) grain size shows that it is more likely (40%) not to pick up this grain size at all (1% of the sample weight) in comparison with the previous settings. This probability was closer to 30% and 20% for the closed and the control settings, respectively. As shown in the CDFs and heatmaps, the bootstrap distributions spread out more evenly over a longer range of sample weight. Moreover, there is a spike in the intensity for the largest grain size (Figure 8, bottom row), which is indicated by the dark blue bar in the original sample and the light blue bar in the bootstrap sample.

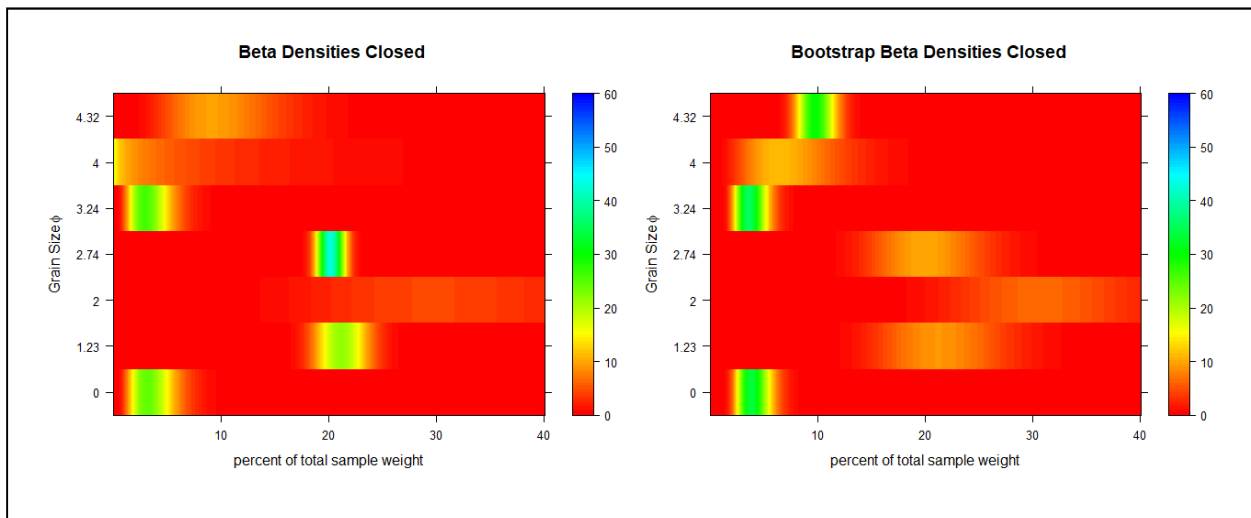


Figure 6. Closed test—heat maps of original samples and bootstrap samples.

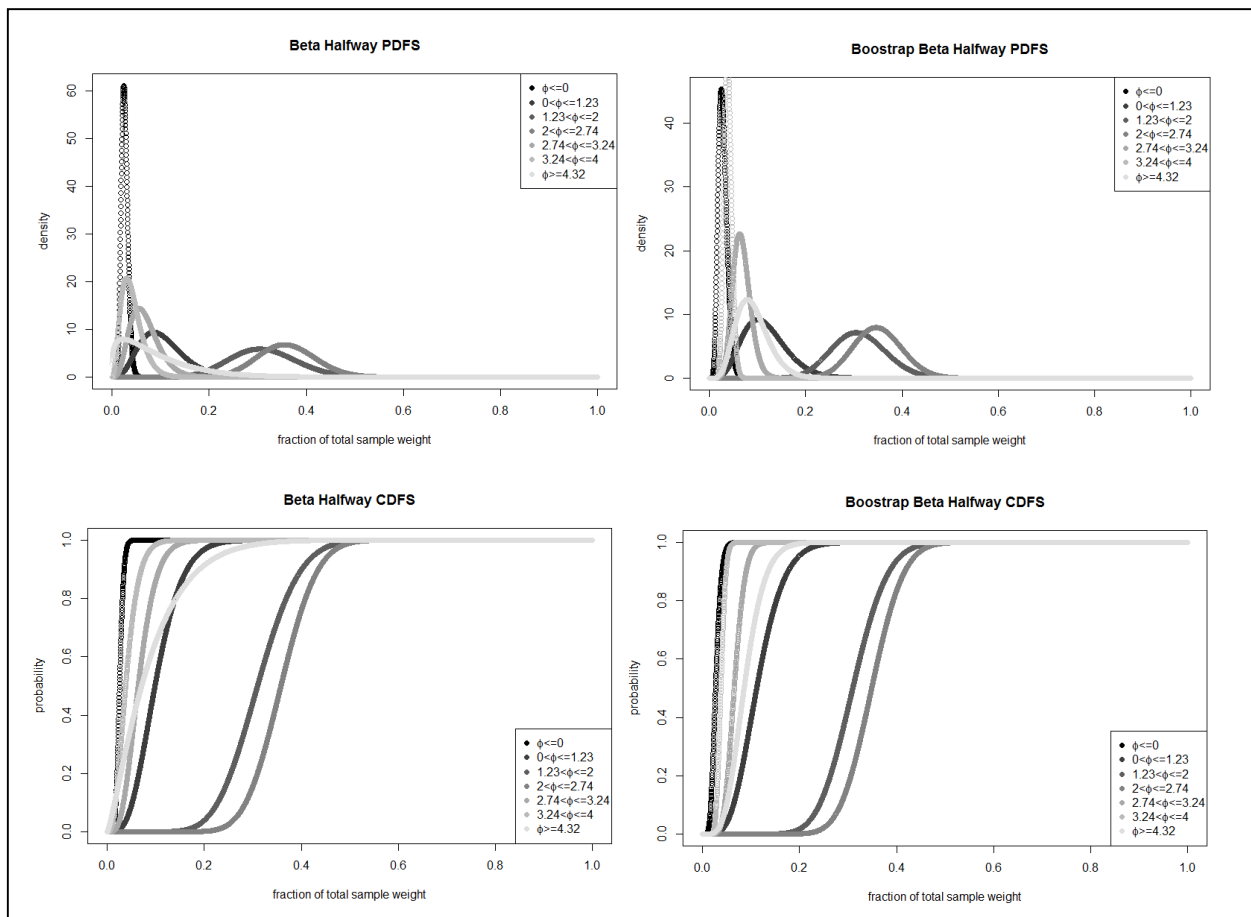


Figure 7. Halfway design setting—beta distributions of original samples along with bootstrap distributions.

Although the intensity of the bootstrap spike is reduced in comparison with the intensity of the original sample for the very large grain size, it has a slightly broader spread. In contrast, a bootstrap spike can be observed for the relatively small grain size, which does not appear in the heatmap of the original sample.

Finally, looking at the open setting, Figures 9 and 10 show much different results compared to what was observed for the other test settings. The probability of not picking

up the very large grain size (weight percentage close to zero) is about 50% in this setting, as there is a 50% chance (CDF in Figure 9) that the very large grain size makes up just over 0% of the total sample weight. The bootstrap distributions are comparatively similar to the distributions of the original samples, but they spread out over a broader range of sample weight. The difference is substantial for the medium grain size depicted in Figures 9 and 10. From the heatmap, it is noted that the medium grain size has a sharper intensity over a shorter length, while the bootstrap distribution has a dimmer intensity over a longer range. This difference for the medium grain size can be observed as a shift in the CDF from an impulse at about 40% of the total sample weight to a smoother increase between 30% and 45% of the sample weight in the bootstrap distribution. The differences between the distributions of the original and the bootstrap samples are more clearly illustrated in Figure 10. For instance, the spike intensity peak for the very large grain size is shifted slightly to the right in the bootstrap, representing a larger fraction of the sample weight.

Reviewing the heat maps in Figure 4, Figure 6, Figure 8, and Figure 10 suggest that in almost all settings, the intensities of the smaller grain sizes, including small, relatively small, and very small (except for the very small grain size in the control test), become steeper. Moreover, the peak of the medium grain size is typically associated with a larger percentage of the total sample weight, and its bootstrap distribution is somewhat stretched in comparison with the distribution of the original samples in all settings except for the halfway test. In comparison with the distribution of the original samples, the bootstrap distribution of the large grain size is steepened except for in the control test. In comparison with the other grain sizes though, the distribution peak is substantially lower, and the distribution is spread across a broader range of sample weight. This demonstrates that there is more fluctuation on how much of the sample weight will be made up of a large grain size. Meanwhile, the bootstrap distribution of the relatively large grain size is flattened in all tests except for the open setting. Similarly, the bootstrap distribution of the very large grain size is flattened in all settings except for the open setting.

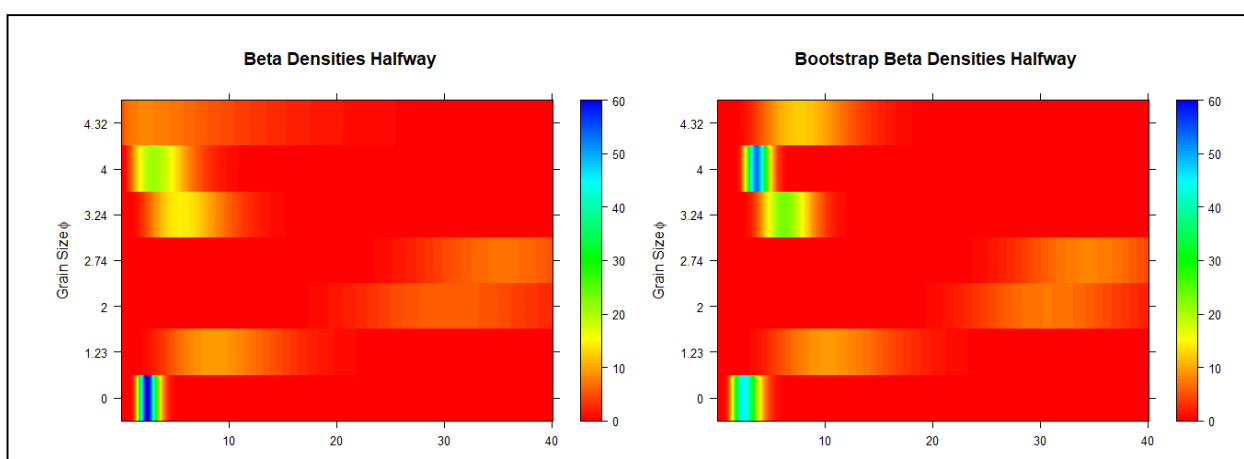


**Figure 8.** Halfway test—heat maps of original samples and bootstrap samples.

We also visualized the weight distribution for different grain sizes using the boxplot. Results are depicted in Figure 11. By visual inspection, we can notice the difference in the mean weight for different grain sizes in all settings, including control, closed, halfway, and open. To investigate the statistical significance of mean weight differences for the different grain sizes, we used Tukey's 'Honest Significant Difference' method. In this way, a set of confidence intervals were constructed for the differences between the means of different grain sizes with the specified family-wise probability of coverage where the intervals are based on the studentized range statistic. As we can observe in Figure 12, no confidence interval contains zero, rejecting the null hypothesis that any given pair of grain sizes have the same mean weight. Lower bound, upper bound, and p-value

for all confidence intervals for the different settings are reported in four tables in the Supplementary Materials. Careful interpretation of the heatmaps and Tukey’s confidence intervals suggests significant differences in the weight proportion of each grain size. We must point out that while heat maps visualize the weight percentage of each grain size, Tukey’s confidence intervals demonstrate the difference in the mean weight percentages of the different grain sizes.

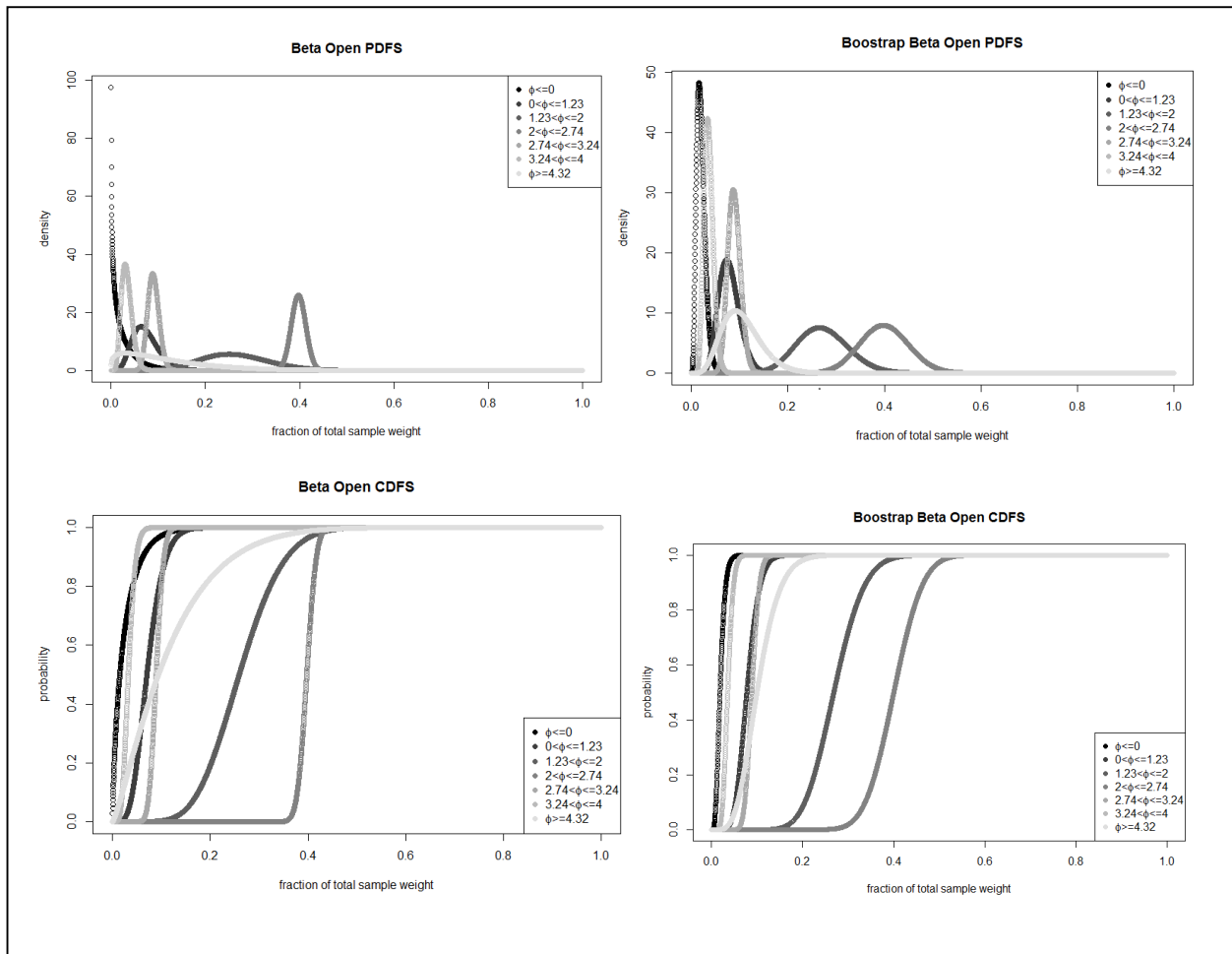


Figure 9. Open design setting—beta distributions of original samples along with bootstrap distributions.

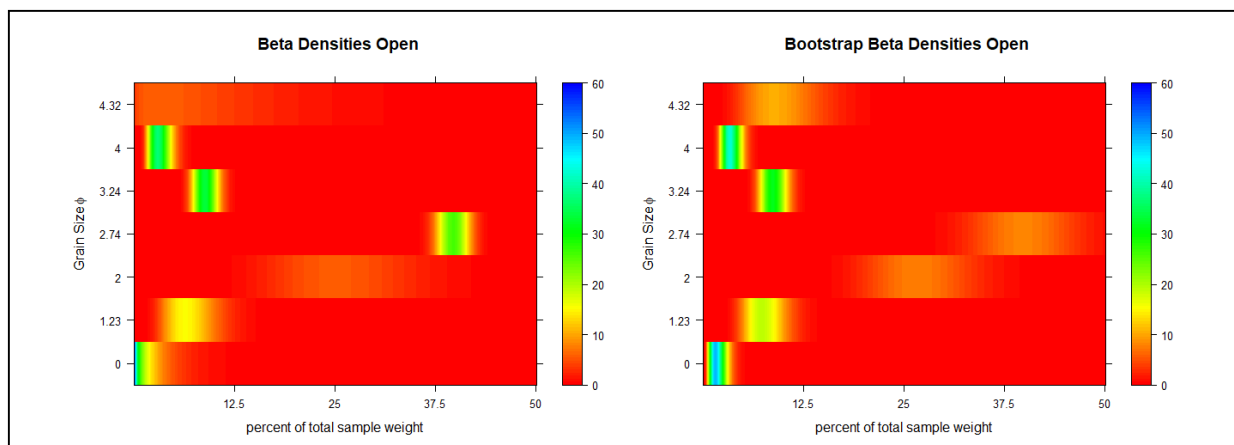


Figure 10. Open test—heat maps of original samples and bootstrap samples.

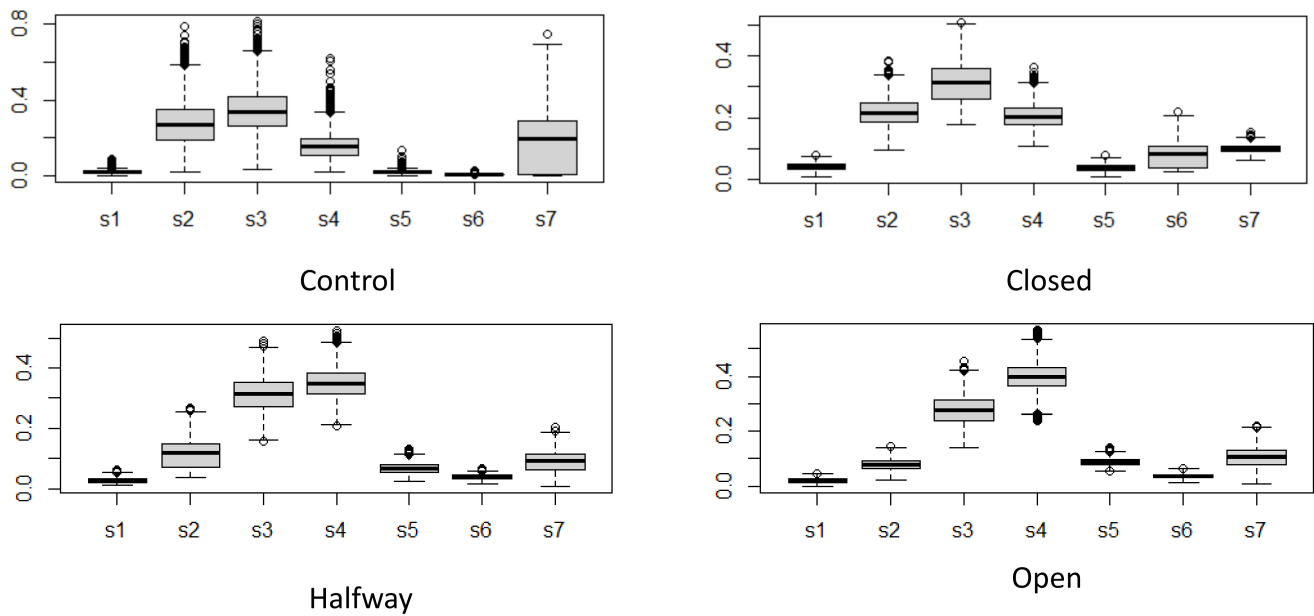


Figure 11. Box plot of proportion of sediment weights for different grain sizes.

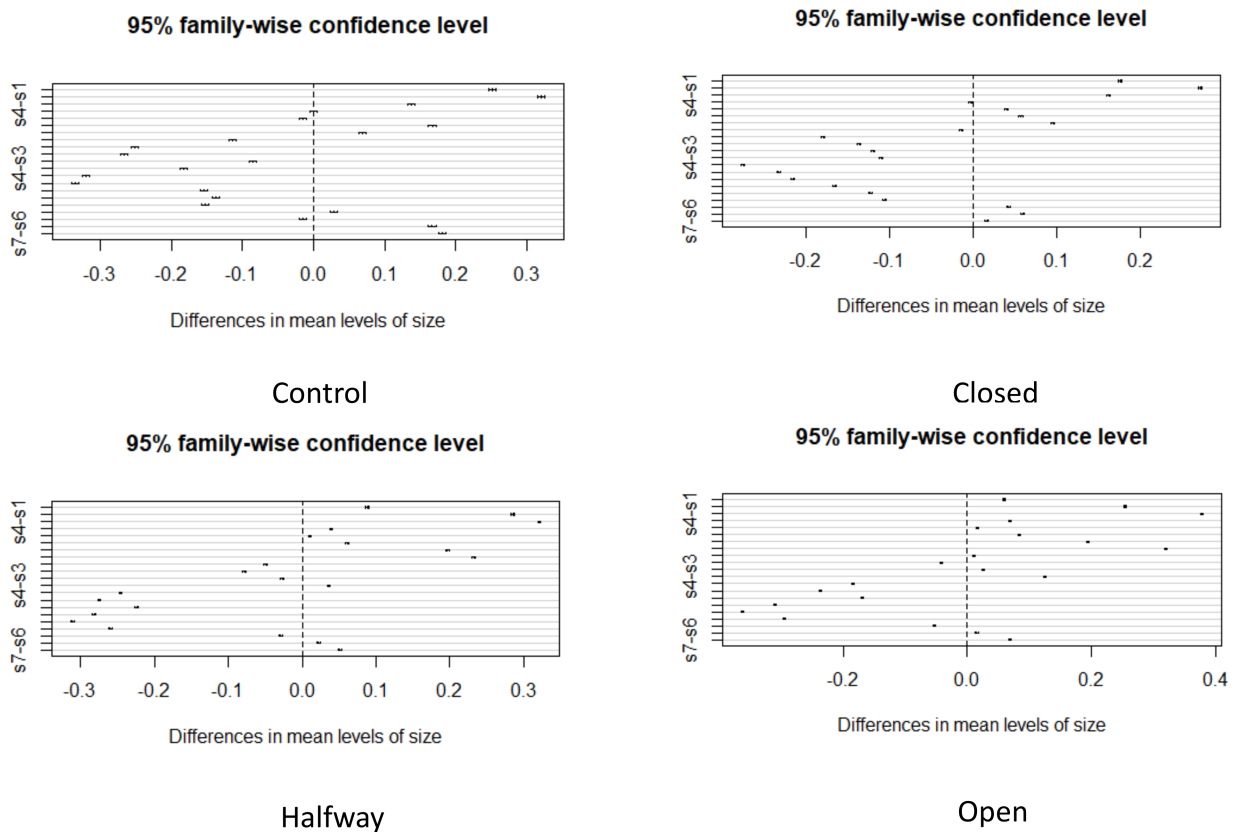


Figure 12. Family-wise confidence interval of proportion of sediment weights for different grain sizes.

### 5. Summary and Conclusions

In this work, a surgical dredging method with a variable area suction head was used for the dredging of fine sediment. The variable area suction head can easily maneuver around the docks, pilings, and other infrastructures to isolate the fine grain material and

better manage the dredged volumes in the seabed. Several samples were collected with different design settings. Collected samples for each design set were used to model the distribution of different grain sizes in the dredged sediments. The proposed statistical model can be used to improve the design efficiency by predicting the sediment sampling outcomes regarding the gradation of the fine sediments. The sediments were divided into seven groups based on the grain size, from very small to very large. Four test designs, including three different suction head settings along with a control test, were performed. The collected data in each test were used to model a probability distribution for each grain size separately. In this way, seven distributions were modeled for each suction head setting. Due to the limited resources, our sample size for each setting was small. Therefore, a bootstrap analysis was performed to virtually generate larger samples.

Ultimately, the estimated distributions can be employed to estimate distributions of grain size in the dredged sediments by adjusting the suction head settings. In turn, dredge operators can optimize the design of the suction to suit a distribution that is skewed more toward our desired results. Our future work will be focused on using the estimated distributions to optimize the dredging performance and use the collected samples to tune the distribution of each grain size.

**Supplementary Materials:** The following are available online at <https://www.mdpi.com/article/10.3390/hydrology8030098/s1>, Tables S1 to S3: Bootstrap Tables, Tables S4 to S7: Tukey's 'Honest Significant Difference'.

**Author Contributions:** Conceptualization, N.N.K., L.A.P. and R.W.; methodology, N.N.K., L.A.P. and R.W.; software, L.A.P. and N.N.K.; validation, N.N.K. and L.A.P.; formal analysis, L.A.P. and N.N.K.; investigation, L.A.P., N.N.K. and R.W.; data curation, L.A.P. and R.W.; writing—original draft preparation, L.A.P., N.N.K. and R.W.; writing—review and editing, N.N.K., L.A.P. and, R.W.; visualization, N.N.K. and L.A.P.; supervision, N.N.K.; project administration, R.W. and N.N.K. All authors have read and agreed to the published version of the manuscript.

**Funding:** This research received no external funding.

**Institutional Review Board Statement:** Not applicable.

**Informed Consent Statement:** Not applicable.

**Data Availability Statement:** The dataset used in this research is included in this paper in the online Supplementary Section.

**Conflicts of Interest:** The authors declare no conflict of interest.

## References

1. Environmental Protection Agency. Climate Adaptation and Water Quality. 2020. Available online: <https://www.epa.gov/arc-x/climate-adaptation-and-water-quality> (accessed on 28 June 2021).
2. World Meteorological Organization (WMO). Climate Change and Desertification. *WMO Publication*. 2007. Available online: [https://library.wmo.int/doc\\_num.php?explnum\\_id=5047](https://library.wmo.int/doc_num.php?explnum_id=5047) (accessed on 28 June 2021).
3. NOAA. National Climate Report—Annual. NOAA National Centers for Environmental Information. 2017. Available online: <https://www.ncdc.noaa.gov/sotc/national/201613> (accessed on 28 June 2021).
4. Yasarer, L.M.; Bingner, R.L.; Garbrecht, J.D.; Locke, M.A.; Lizotte, R.E., Jr.; Momm, H.G.; Busted, P.R. Climate change impacts on runoff, sediment, and nutrient loads in an agricultural watershed in the Lower Mississippi River Basin. *Appl. Eng. Agric.* **2017**, *33*, 379–392. [[CrossRef](#)]
5. Hovenga, P.; Wang, D.; Medeiros, S.; Hagen, S.; Alizad, K. The Response of Runoff and Sediment Loading in the Apalachicola River, Florida to Climate and Land Use Land Cover Change. *AGU Publ.* **2016**. [[CrossRef](#)]
6. Jeppesen, E.; Kronvang, B.; Meerhoff, M.; Søndergaard, M.; Hansen, K.; Andersen, H.; Lauridsen, T.; Liboriussen, L.; Beklioglu, M.; Özen, A.; et al. Climate Change Effects on Runoff, Catchment Phosphorus Loading and Lake Ecological State, and Potential Adaptations. *J. Environ. Qual.* **2009**, *38*, 1930–1941. [[CrossRef](#)] [[PubMed](#)]
7. Shrestha, R.R.; Dibike, Y.B.; Prowse, T.D. Modeling Climate Change Impacts on Hydrology and Nutrient Loading in the Upper Assiniboine Catchment. *J. Am. Water Resour. Assoc. (JAWRA)* **2011**, *48*, 74–89. [[CrossRef](#)]
8. Arheimer, B.; Andréasson, J.; Fogelberg, S.; Johnsson, H.; Pers, C.B.; Persson, K. Climate Change Impact on Water Quality: Model Results from Southern Sweden. *AMBIO J. Hum. Environ.* **2005**, *34*, 559–566. [[CrossRef](#)]
9. Florida Sea Grant. *Muck Removal in the Save Our Indian River Lagoon Project Plan*; Fact Sheet: Gainesville, FL, USA, 2017.

10. Trefry, J.H.; Fox, A.L.; Trocine, R.P.; Fox, S.L.; Voelker, J.E. Determining the Effectiveness of Muck Removal on Sediment and Water Quality in the Indian River Lagoon, Impacts of Environmental Muck Dredging 2016-2017 Determining the Effectiveness of Muck Removal on Sediment and Water Quality in the Indian River Lag. December 2017. Available online: <https://www.fit.edu/indian-river-lagoon/> (accessed on 28 June 2021).
11. Trefry, J.H.; Johnson, K.B.; Shenker, J.; Zarillo, G.A. *Impacts of Environmental Muck Dredging*; Florida Institute of Technology: Viera, FL, USA, 2016.
12. Trefry, J.H.; Metz, S.; Trocine, R.P.; Iricanin, N.; Burnside, D.; Chen, N.; Webb, B. *Design and Operation of a Muck Sediment Survey*; Dept of Oceanography and Ocean Engineering, Florida Institute of Technology: Melbourne, FL, USA, 1990.
13. Fox, A.; Trefry, J. Environmental Dredging to Remove Fine-Grained, Organic-Rich Sediments and Reduce Inputs of Nitrogen and Phosphorus to a Subtropical Estuary. *Mar. Technol. Soc.* **2018**, *52*, 42–57. [[CrossRef](#)]
14. Tetra Tech Inc.; CloseWaters LLC. Revised Save Our Indian River Lagoon Project Plan 2019 Update for Brevard County, Florida. 2019. Available online: <https://www.dropbox.com/s/j9pxd59mt1baf7q/Revised2019SaveOurIndianRiverLagoonProjectPlanUpdate032519.pdf?dl=0> (accessed on 28 June 2021).
15. Barile, P.J. Widespread sewage pollution of the Indian River Lagoon system, Florida (USA) resolved by spatial analyses of macroalgal biogeochemistry. *Mar. Pollut. Bull.* **2018**, *128*, 557–574. [[CrossRef](#)] [[PubMed](#)]
16. Palermo, M.; Schroeder, P.; Estes, T.; Francingues, N. *Technical Guidelines for Environmental Dredging of Contaminated Sediments*; Army Corps of Engineers Engineering Research and Development Center: Vicksburg, MS, USA, 2008.
17. Maglio, C.; Weaver, R.; Trefry, J.; Bostater, C.; Shenker, J.; Johnson, K.; Trulock, S.; Ousley, J.; Cotter, P.; DeMarco, P.M.; et al. Environmental benefits realized during navigation maintenance dredging: A Case Study in the Indian River Lagoon, Florida. *WEDA J. Dredg.* **2021**, *19*, 1–13.
18. Newell, R.C.; Seiderer, L.J.; Hitchcock, D.R. *The Impact of Dredging Works in Coastal Waters: A Review of the Sensitivity to Disturbance and Subsequent Recovery of Biological Resources on the Sea Bed, Oceanography and Marine Biology: An Annual Review*; UCL Press, University College London (UCL): London, UK, 1998; Volume 36, pp. 127–178.
19. Weaver, R.; Waite, T.; Grisanti, H.; Provost, L. *Feasibility of Muck Removal in the IRL Watershed and Subsequent Ferrate Treatment to Remove Excess Nutrients*; Florida Institute of Technology, Brevard County Natural Resources Management Department: Melbourne, FL, USA, 2018.
20. Provost, L.A.; Waite, T.D.; Weaver, R.J.; Grisanti, H.C. Fabrication and Testing of a Variable Area Dredge Coupled with an Inline Slurry Treatment System. *Mar. Technol. Soc. J.* **2018**, *52*, 75–80. [[CrossRef](#)]
21. Dean, R.; Dalrymple, R. *Coastal Processes*; Cambridge University Press: Cambridge, UK, 2004.
22. United States. *Coastal Engineering Manual*; EM 1110-2-1100 (Part III); U.S. Army Corps of Engineers: Washington, DC, USA, 2002.
23. Inman, D.L. Measures for Describing the Size Distributions of Sediments. *J. Sediment. Petrol.* **1952**, *22*, 125–145.
24. Gupta, A.; Nadarajah, S. *Handbook of Beta Distribution and Its Applications*; Marcel Dekker: New York, NY, USA, 2004.
25. Devore, J. *Probability and Statistics for Engineering and the Sciences*, 9th ed.; International Metric Edition; Cengage Learning: Boston, MA, USA, 2016.
26. Hogg, R.; Tanis, E.; Zimmerman, D. *Probability and Statistical Inference*, 9th ed.; Pearson: London, UK, 2015; p. 303.